Reflection of Planar Shock Waves from Rubber Walls: Uniaxial Strain Case

G. Ben-Dor,* G. Mazor,† M. Mond,‡ and O. Igra*
Ben-Gurion University of the Negev, Beer Sheva, Israel
and
W. Heilig§ and H. Reichenbach¶
Ernst Mach Institute, Freiburg, Germany

Introduction

MAZOR et al.[1] recently published a comprehensive study in which the head-on-reflection of a planar shock wave from a rubber-supported flat plate was investigated analytically, numerically, and experimentally. They pointed out in their study that the reflection process depends on the degrees of freedom of the supporting rubber to expand in the x, y, and z directions.

Consider Fig. 1, where the considered problem is schematically illustrated. As shown in the bottom part of that figure, there are three modes of compression that could be experienced by the rubber:

1) A uniaxial stress mode in which the rubber is free to expand in both the y and z directions and hence can develop stresses only in the x direction. Consequently, for this mode of compression $\sigma_x \neq 0$, $\sigma_y = 0$, $\sigma_z = 0$, $\epsilon_x \neq 0$, $\epsilon_y \neq 0$, and $\epsilon_z \neq 0$.

2) A biaxial stress mode in which the rubber is free to expand only in its z direction and hence can develop stresses both in the x and y directions. Consequently, for this mode of compression $\sigma_x \neq 0$, $\sigma_y \neq 0$, $\sigma_z = 0$, $\epsilon_x \neq 0$, $\epsilon_y = 0$, and $\epsilon_z \neq 0$.

3) A uniaxial strain (also referred to as triaxial stress) mode in which the rubber cannot expand either in the y or the z directions and hence develops stresses in the x, y, and z directions. Consequently, for this mode of compression $\sigma_x \neq 0$, $\sigma_y \neq 0$, $\sigma_z \neq 0$, $\epsilon_x \neq 0$, $\epsilon_y = 0$, and $\epsilon_z = 0$.

Detailed derivation of the governing equations of the problem under consideration is given in Ref. 1 together with a list of the equations in nondimensionalized form. Consequently, only the assumptions upon which the governing equations and their solutions are based are given here. They are the following:

1) The flow is one dimensional.
2) The gas is an ideal fluid.
3) The gas behaves as a perfect gas.
4) The gravitational force is negligibly small.
5) The rubber is perfectly elastic, isotropic, and incompressible.
6) The changes in the internal energy of the rubber are negligibly small.
7) The stresses that develop in the rubber are uniformly distributed along any cross-sectional area perpendicular to the x axis; therefore the rubber's cross-sectional area remains planar throughout the compression process.
8) The cross section of the rubber is uniform.
9) The transverse dimensions of the rubber are small with respect to the longitudinal dimensions.
10) The rubber does not buckle under the compressive loads.

The final set of the governing equations, in a Lagrangian form, consists of 10 equations, namely, 1) conservation of mass in the gaseous phase, 2) definition of the gas particles' velocity, 3) conservation of linear momentum in the gaseous phase, 4) conservation of energy in the gaseous phase, 5) equation of state for the gaseous phase, 6) conservation of mass in the rubber, 7) definition of the rubber particles' velocity, 8) definition of the extension ratio in the rubber, 9) conservation of linear momentum in the rubber, and 10) the constitutive (stress-strain) relation for the rubber.

The set of governing equations that consisted of 10 dependent variables, and hence was solvable in principle, was transformed into a set of central finite difference equations. The set of finite difference equations was solved with second-order accuracy using the artificial viscosity technique. More details about the numerical solution can be found in Ref. 2.

The experimental investigation of the problem under consideration in the case of a biaxial stress mode of compression was reported in detail in Ref. 1. Hence, the purpose of the present Note is to report on our experimental investigation in the case of a uniaxial strain mode of compression.

Present Study

Unlike the uniaxial stress and biaxial stress modes of compression that have stress-strain relations that are available in the open literature, a similar relation for the uniaxial strain mode of compression does not exist. As a consequence, in the course of the present study, the following stress-strain relation was developed for the case of a uniaxial strain compression mode:

$$\sigma_x = \frac{2G(1+\nu)}{1-2\nu^2/(1-\nu)}(\lambda_x - 1) \tag{1}$$

where σ_x is the stress in the x direction, λ_x is the extension ratio in the x direction (note that $\lambda_x = 1 - \epsilon_x$ where ϵ_x is the strain in the x direction, for compressive loads $0 < \lambda_x < 1$), ν is Poisson's ratio, and G is the elasticity constant.

It should be noted here that, as shown in Fig. 1, the uniaxial strain compression mode cannot satisfy by definition the assumption of an incompressible rubber since in this case $\epsilon_x \neq 0$, $\epsilon_y = \epsilon_z = 0$, and hence the volume of the rubber changes whereas its mass remains constant. As a consequence, Eq. (1) is limited to small deformations only, i.e., small values of ϵ_x. This limitation ensures that the total change in the volume of the rubber is small enough to assume that its density remains constant.

Experimental Results

The experimental setup for obtaining the uniaxial strain compression mode is shown in Fig. 2. The cross section of the

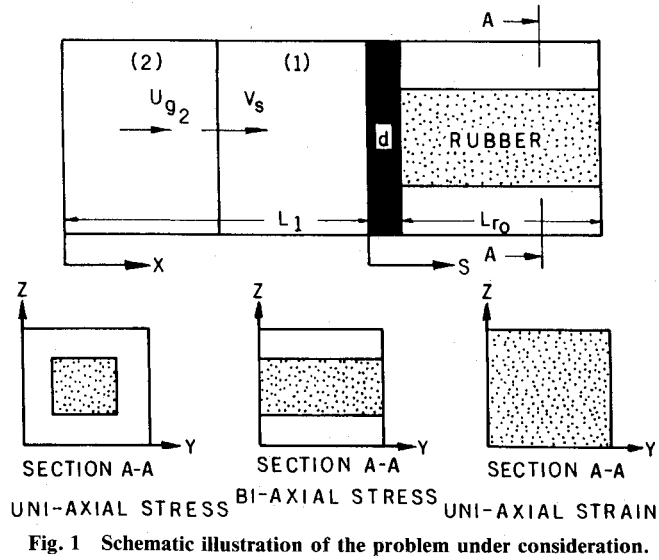

Fig. 1 Schematic illustration of the problem under consideration.

Received May 6, 1992; revision received April 26, 1993; accepted for publication May 7, 1993.

*Professor, Department of Mechanical Engineering, Pearlstone Center for Aeronautical Engineering Studies.
†Postdoctoral Fellow, Department of Mechanical Engineering, Pearlstone Center for Aeronautical Engineering Studies.
‡Associate Professor, Department of Mechanical Engineering, Pearlstone Center for Aeronautical Engineering Studies.
§Senior Researcher.
¶Retired.

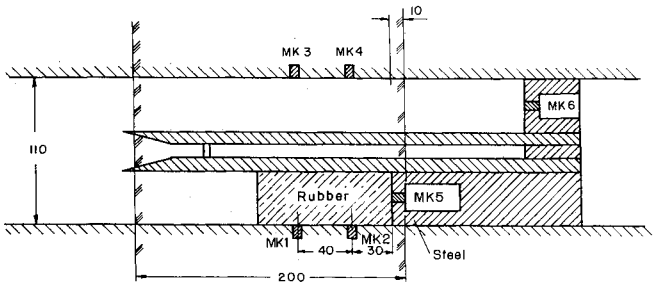

Fig. 2 Experimental setup for the uniaxial strain compression.

rubber rod was 4 × 4 cm, and its initial length was 10 cm. Its initial density ρ_{r_0} was 1007 kg/m^3, and its chemical composition was 100.0 g natural rubber, 2.0 g stearine, 5.0 g zink oxide, 10.0 g carbon black haf, 2.0 g antioxidant 224b, 2.75 g sulfur, 1.0 g cyclohexyl benzothiozol sulfenamide (CBS), and 0.1 g tetra methyl thivram disulfide (TMTD). This composition ensured good elasticity. To have a good estimation of the elasticity constant of the rubber, it was compressed in an Instron machine under a biaxial loading mode. The experimental results were fitted to a curve of the form $\sigma = G(\lambda - 1/\lambda^3)$, which is the form of the stress-strain relation for a biaxial compression mode. The maximum deviation of the experimental results from a curve having a value of $G = 931{,}667$ N/m^2 was less than 5%.

Based on Nowinski,[3] compression waves, generated in a solid material, will converge to a shock wave if the stress-strain relation of the material fulfills the following two requirements:

$$\frac{\partial \sigma_x}{\partial \lambda_x} > 0 \tag{2a}$$

$$\frac{\partial^2 \sigma_x}{\partial \lambda_x^2} > 0 \tag{2b}$$

From the stress-strain relation of a rubber [see Eq. (1)], it is clear that the requirements given by Eqs. (2a) and (2b) are not fulfilled, and hence the compression waves are not expected to converge to a shock wave in a uniaxial strain mode of compression.

The stresses developing in the rubber rod were measured using Kistler piezoelectric pressure transducers at three different locations that are marked in Fig. 2 as MK1, MK2, and MK5 and are located 3, 7, and 10 cm, respectively, from the front of the rubber rod.

The stress histories as recorded at these three locations, i.e., MK1, MK2, and MK5, for an incident shock wave Mach number $M_s = 1.54$, an initial pressure $P_0 = 0.985$ bar, and an initial temperature of $T_0 = 292.5$ K are shown in Figs. 3a–3c, respectively. The stress histories at MK1, MK2, and MK5 clearly indicate that the compression waves did not converge to a shock wave. Furthermore, it is seen that the waves move faster in reality (the actual experiment) as compared with the numerical simulation. (Note that the solid lines start to rise earlier than the dashed lines.) The wave propagation velocity c_0 can be calculated from[4]

$$c_0^2 = \frac{1}{\rho_{r_0}} \frac{\partial \sigma_x}{\partial \lambda_x} \tag{3}$$

where ρ_{r_0} is the initial density of the rubber (note that under the assumption that the rubber is incompressible its density remains constant).

Using this relation together with Eq. (1) clearly indicates that in the present case

$$c_0^2 = \frac{2G}{\rho_{r_0}} \frac{1+\nu}{1 - 2\nu^2/(1-\nu)} \tag{4}$$

Consequently, based on the foregoing discussion, it could be concluded that the value used in the numerical simulation for the elasticity constant G is smaller than the actual one.

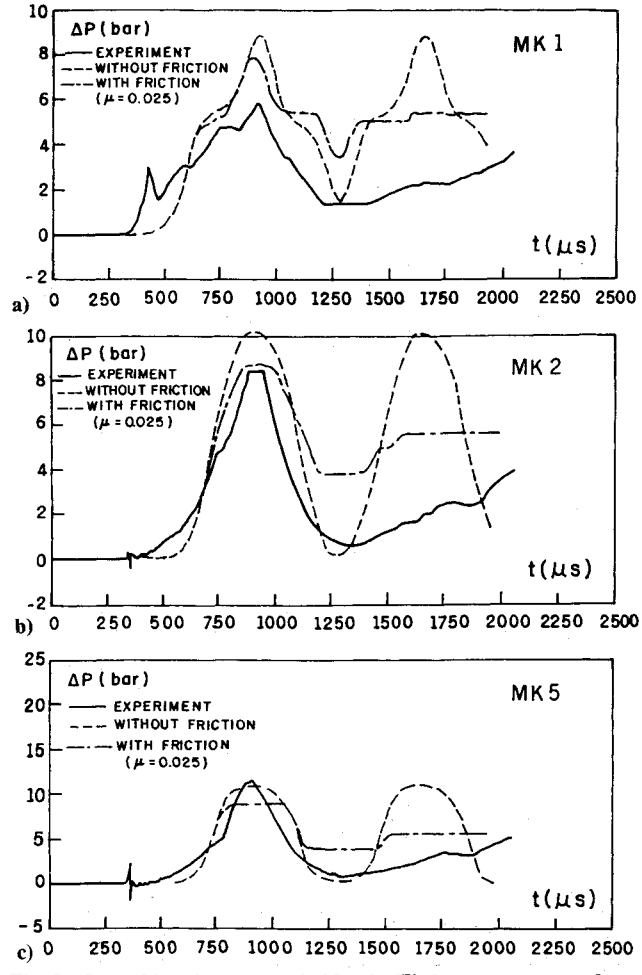

Fig. 3 Stress histories as recorded by the Kistler pressure transducers that were mounted at a) MK1, b) MK2, and c) MK5 (see Fig. 2).

This could be due to the fact that the value of G, as used in the numerical simulation, was obtained from a biaxial stress static compression experiment, whereas the actual loading process is a uniaxial strain compression mode and dynamic.

As can be seen in Figs. 3a–3c, two numerical simulations were conducted, the first neglecting the friction between the rubber rod and the solid sufaces that bounded it, the second accounting for the friction by means of a simplified model for which the coefficient of friction was chosen to be $\mu = 0.025$. Although the peak stress value in Fig. 3a is seen to be smaller than the numerically predicted one, the peak stress values in Figs. 3b and 3c are seen to be predicted quite well. The peak over stresses (i.e., $P - P_0$, where $P_0 = 0.085$ bar) as measured in stations MK1, MK2, and MK5 are 5.8, 8.35, and 11.44 bars, respectively. (Note that there is a saturation in the recorded stress in Fig. 2b; hence the actual stress is somewhat larger than the recorded plateau.) Consequently, the peak stresses in these stations are 6.785, 9.335, and 12.425 bars, respectively.

The peak pressure at MK5 clearly indicates that the pressure acting on the end wall of the shock tube is significantly enhanced due to the presence of the rubber rod. Note that had the incident shock wave reflected head on directly from the endwall, the pressure at the endwall would be 5.897 bars. Hence, the pressure at the endwall is more than doubled due to the presence of the rubber.

It is also important to note that, although the numerically predicted stress profiles do not simulate the actual profiles well enough, the time durations of the stress pulses are very well simulated at all three locations. Note that due to the extremely strong dumping mechanism that is involved in the actual experiment, only the first loading cycle could be simulated using our simplifying physical model. Note also that when friction is not accounted for, the numerical simulations

are seen to have a repeating cycle. However, the inclusion of friction induces a decaying mechanism that results in a better agreement with the experimental results. (Compare the dashed and the dashed-dotted lines.)

Conclusions

The head-on reflection of a planar shock wave from a rubber wall experiencing a uniaxial strain loading mode that was investigated numerically during a previous study[1] was compared with experimental results that were obtained recently.

It has been demonstrated that Kistler piezoelectric pressure transducers could be used to record stresses in rubberlike materials, although they originally were designed to measure pressures in fluids.

In view of the previous remark, the comparison of the actual experimental results with the numerical simulations revealed a very good agreement as far as the durations of the stress pulses are involved and fairly good agreements as far as the shapes and peak values of the stress pulses are concerned.

Finally, the conclusions from the numerical investigation[1] that rubberlike materials cannot be used to reduce head-on reflecting shock wave loads on structure have been verified experimentally. Both the numercial and the experimental investigations clearly indicate that the presence of the rubber results in a significant amplification of the pressure acting on the endwall of the shock tube. Consequently, experimental setups similar to that shown in Fig. 1 could be used as pressure amplifiers.

Acknowledgment

This research was supported by a grant from the German-Israeli Foundation for Scientific Research and Development. Its support is acknowledged with thanks.

References

[1]Mazor, G., Igra, O., Ben-Dor, G., Mond, M., and Reichenbach, H., "Head-On Collision of Normal Shock Waves with a Rubber Supported Wall," *Transactions of the Royal Society of London,* Series A, 1992, pp. 237–269.

[2]Mazor, G., "The Influence of Surface Properties on the Head-On Reflection of Shock Waves," Ph.D. Thesis, Dept. of Mechanical Engineering, Ben-Gurion Univ. of the Negev, Beer Sheva, Israel, 1989.

[3]Nowinski, J. L., "On the Propagation of Finite Disturbances in Bars of Rubberlike Materials," *Journal of Engineering Industry,* Vol. 87, 1965, pp. 523–529.

[4]Courant, R., and Friedrichs, K. O., *Supersonic Flow and Shock Waves,* Interscience, New York, 1948.

Large Displacement Axisymmetric Element For Nonaxisymmetric Deformation

T. M. V. Kaiser*
Centre for Frontier Engineering Research, Edmonton, Alberta T6N 1E2, Canada
and
A. E. Elwi† and A. Mioduchowski‡
University of Alberta, Edmonton, Alberta T6G 2G8, Canada

I. Introduction

LARGE deformation, three-dimensional analyses of axisymmetrical structures can be costly in spite of the relatively simple geometry. One approach to efficiently analyzing such problems is to use axisymmetric elements that are formulated to allow for nonaxisymmetric deformations. A cylindrical coordinate system in the context of a total Lagrangian formulation seems appropriate for these elements.

Although many programs use cylindrical, spherical, or local coordinate systems for input convenience, the underlying formulation is usually based on Cartesian reference systems.[1–3] Although significant efforts have been devoted to cylindrical formulations, most efforts have been restricted to small displacements[4,5] or shell elements.[6–11]

This Note discusses a Lagrangian finite element formulation in general orthogonal curvilinear coordinate systems, including the basic components describing Lagrangian strains and strain increments and the procedure for integrating these into the virtual work equation. This generalized formulation is applied to a solid cylindrical finite element that is demonstrated at the end of this Note. Although developed to address structural problems in the oil industry, the formulation developed herein is general with much broader application potential.

II. Lagrangian Strains in Curvilinear Coordinates

Lagrangian formulations use the Green-Lagrange strains because they have the desirable characteristic of remaining invariant under rigid-body rotation. Many authors express Green-Lagrange strains in terms of the deformation gradient in general curvilinear or orthogonal curvilinear coordinate systems.[1,12–14] The development that follows is based largely on Malvern's discussion.[12] In orthogonal coordinate systems, the covariant and contravariant components are coincident, and so only one component type needs to be considered. Therefore, the convention of summation for repeated subscripts is used in this Note.

The spatial components of the material vector may be expressed in terms of the material components through the deformation gradient tensor F_{km}:

$$\mathrm{d}s_k = \frac{h^k}{h^m}\left(\frac{\partial x_k}{\partial X_m}\right)\mathrm{d}S_m = F_{km}\,\mathrm{d}S_m \tag{1}$$

This can be substituted into the expression for the Green-Lagrange strains, giving

$$E_{ij} = \frac{1}{2}\left[\frac{(h^k)^2}{H^i H^j}\frac{\partial x_k}{\partial X_i}\frac{\partial x_k}{\partial X_j} - \delta_{ij}\right] \tag{2}$$

In finite element applications the strains must be expressed in terms of the displacement field. This requires appropriate displacement measures to be defined. Although Cartesian scale factors are independent of location and displacements, in curvilinear coordinate systems location-dependent scale functions add considerable complexity. At this point most authors simplify their discussions to infinitesimal strain formulations,[12,13] so that physical displacements can be used as field variables, and the scale functions can be assumed to be constant.

Defining physical displacements that include deformation-dependent scale functions is more difficult and unnecessary. Instead, coordinate displacements can be used as the field variables. This approach was used by Truesdell and Toupin[14] for Lagrangian strains in general curvilinear coordinate systems; however, it has not previously been used in incremental form for a finite element formulation. The displacements are defined simply as

$$u_i = x_i - X_i \tag{3}$$

where $i = r, \theta, z$ in a cylindrical system.

The strains can then be expressed in terms of the displacement field and scale functions:

$$E_{ij} = \frac{1}{2H^i H^j}\left(h^{j^2}u_{j,i} + h^{i^2}u_{i,j} + h^{k^2}u_{k,j}u_{k,i} - h^{k^2}\delta_{kj}\delta_{ki} - \delta_{ij}\right) \tag{4}$$

The displacement gradient components in the first three terms are similar to the usual Cartesian expressions. The last two terms

Received March 28, 1992; revision received March 26, 1993; accepted for publication March 26, 1993.

*Research Engineer, 200 Karl Clark Road.
†Professor, Department of Civil Engineering.
‡Professor, Department of Mechanical Engineering.